Optimization of Acoustic Metasurfaces with Hybrid Structures for attenuation of broadband low frequency sound

An exploratory research on hybrid metamaterials to analyze/uncover possible practical applications/benefits for sound attenuation

Master's Thesis

Carlos Martínez Fornos

Delft University of Technology

TUDelft

Optimization of Acoustic Metasurfaces with Hybrid Structures for attenuation of broadband low frequency sound

An exploratory research on hybrid metamaterials to analyze/uncover possible practical applications/benefits for sound attenuation

by

Carlos Martínez Fornos

Student Name	Student Number
Martínez Fornos Carlos	5333547

Supervisor: Alejandro M. Aragón
Supervisor: Marcel Sluiter
Project Duration: June, 2022 - March, 2024
Faculty: Faculty of Mechanical, Maritime and Materials Engineering (3mE), Delft

Style: TU Delft Report Style, with modifications by Daan Zwaneveld

TUDelft

Acknowledgements

To my supervisor Alejandro M. Aragón for guiding me throughout all this process and encouraging me to do better at every moment.

To my friends back home who gave me strength and support through this journey. To whom more than friends I consider brothers.

To my family for always being there for me unconditionally. Without them none of this would have been possible and I owe the world to them.

Abstract

We perform a study on acoustic metasurfaces, aiming to achieve simultaneously low resonance frequencies (below 400 Hz), high attenuation bandwidth (greater than 200 Hz), and high attenuation coefficient magnitudes (above 0.8), while maintaining a surface-like structure. We propose the implementation of geometrical optimization through genetic algorithms, as well as the incorporation of a chamber to induce resonator coupling in a supercell hexagonal Helmholtz resonator metasurface, to achieve the stated objectives simultaneously. Results show that genetic algorithms can effectively increase the attenuation bandwidth while maintaining a moderate attenuation coefficient magnitude. Incorporating a chamber induces resonator coupling, causing frequency locking and pulling phenomena. A narrow chamber can effectively lower the resonance frequencies and enhance the attenuation coefficients at those frequencies, while maintaining a surface-like structure. However, incorporating a chamber may lead to a reduction in bandwidth. By combining the genetic algorithm optimization with chamber integration, we observe a significant reduction in bandwidth narrowness, while the benefits of frequency locking and pulling are maintained. In conclusion, genetic algorithms have the potential to achieve wide attenuation bandwidths, while chamber incorporation holds promise for attaining low resonance frequencies with high attenuation coefficients. Using both methods simultaneously may enable the achievement of all objectives.

Contents

1

Introduction

Multitonal low frequency noise (MLFN) attenuation is of concern for industries such as aerospace, ground transportation and civil engineering, due to the impact these sound frequencies have on human health [1]. Specifically, the health effects these soundwaves have on the human body range from discomfort and irritability, to hearing loss, sleep disorders, and even cardiovascular diseases [2]. Example of problems that require MLFN attenuation include acoustic liners, which shield from aircraft engine noise [3], and enviromental urban noise inside buildings, all while keeping sufficient inner ventilation [4]. Methods of low frequency noise reduction by use of classical methods include active control techniques [5] and micro perforated panels [6].

The main issue that arises when attempting to attenuate MLFN is the requirement of thicker and heavier structures. Noise attenuation typically happens by scattering and absorption of incident sound waves [7]. Materials follow what is called the mass density law, which states that in order to increase the sound transmission loss of any material by 6 dB, this material needs to double its density or thickness [8]. This law indirectly implies that the lower the frequency of the incoming wave, the less efficient any material will be at attenuating it if the material is too thin. However, increasing the thickness of the material may even become counterproductive due to the phenomenon of critical frequency [8]. At critical frequency, the wavelength of the mechanical bending waves of the material are of the same order as those of the incident sound. The material enters resonance and starts vibrating in phase with the sound, making it loose its attenuation capabilities. The critical frequency of a material decreases as the thickness of the material increases and usable space is crucial in places such as airplanes. For example, in aircrafts, noise attenuating structures occupy space and have considerable weight. This reduces weight carrying capacity and available space, which in turn reduces fuel efficiency, causing economical losses for the industry [9]. In areas such as construction and building design, lighter noise attenuating structures are also needed to avoid reductions in productive and habitable spaces [5]. Not only is it not efficient to increase MLFN attenuation by increasing the material's thickness, but it also makes the material less practical to implement [10]. Therefore increasing the thickness of noise attenuating material is not an option in such cases.

During the early 1980's, materials with special acoustic properties were proposed by Donald A. [11] and Seshadri S. [12]. This proposal gave origin to the study of acoustic scattering structures known as phononic crystals. As an alternative to classical noise attenuating materials, phononic crystals and metamaterials show promise on overcoming the limitations of common sound attenuating materials. Phononic crystals are periodic structures that scatter by means of Bragg's scattering a range of frequency waves (band gap) [13]. Phononic crystals are able to attenuate sound waves with wavelengths of the same scale as the unit structure of the crystal. Their band gap can be analyzed through a band structure analysis. While phononic crystals can display many properties such as wave deflection, reflection and attenuation not possible for regular materials, they are not optimal for MLFN attenuation. Since their crystal unit cell has to be of the same scale as the wavelength they interact with, they need to become big to scatter low frequency sound waves. This doesn't necessarily happens with metamaterials.

Metamaterials, are materials that posses properties that are not usually, or at all, found within regular materials [14]. Metamaterials' characteristic properties are due to their structure, rather than the intrinsic properties of the materials they are made of. The first designed metamaterials were created to display particular properties when interacting with electromagnetic waves. Some of these unique properties include a highly customizable magnetic permeability and electric permittivity, providing the ability to make both their values highly anisotropic, simultaneously negative, or zero [15]. Such properties allow the use of these metamaterials on specialized tasks such as optical cloaking, chemical sensors, and laser accelerators, among others [16].

Almost immediately after electromagnetic/optical metamaterials were introduced, and drawing an analogy from their interaction with electromagnetic waves, metamaterials that interact with mechanical waves were proposed. Such metamaterials are known as acoustic/elastic metamaterials. The fist experimental proposition of an acoustic material was done by Zhengyou Liu et al. [17]. The experiment proposes a double sided acoustic device (a soft rubber sphere composite to be precise) that is able to break the mass density law and attenuate noise of 400 Hz with a dimension of 2 cm. These metamaterials are used for specific tasks such as noise and vibration attenuation [3, 10, 18, 19, 20, 21, 22], wave collimation [23, 24], wave directional transmission [25, 26, 27], cloaking, and total reflection of acoustic/elastic waves [28, 29, 18].

While phononic crystals attribute their unique properties to their periodic structure and Bragg's scattering, the properties of metamaterials are due to local resonance. Local resonance refers to the phenomenon in which subunits within the material material resonate locally in contrast to the overall metamaterial. Acoustic metamaterials are composed of designed unitary substructures termed local resonators. Such structures are usually of milimetric to nanometric scale, and respond in an out-of-phase motion when interacting with elastic or acoustic waves. These resonators are scattered all throughout the material and mechanically behave as a mass-spring oscillator system, embedded within the matrix [30]. When these resonators interact with a wave possessing a coherent frequency to that of the resonator's resonance frequency, they oscillate and produce interference. The cumulative motion of the local resonators opposes that of the sound waves traveling through the material causing destructive interference that effectively attenuates the traveling wave. Acoustic local resonator designs widely researched nowadays include acoustic black holes [21, 31, 32], Mie resonant structures, and Helmholtz resonators [33, 3, 34, 35, 36, 37, 38, 39, 40].

Acoustic metamaterials show properties that make them more optimal than phononic crystals at attenuating low frequency sound. One such property is sub-wavelength sound attenuation, which means that structures with dimensions orders of magnitude smaller than that of the incident sound wavelength can be used for sound attenuation [41]. For example, Meng Jin et al. [41] developed a folded like structure capable of capturing acoustic energy, effectively attenuating incoming sound with metamaterials of sub-wavelength dimensions. Hui Gou et al. [33] proposed a phononic crystal metamaterial hybrid able to resonate with soundwaves, whose wavelength is 4 times bigger than the crystal unit of the phononic crystal. This was done to achieve low frequency energy absorption with piezoelectric elements. The reason these materials can display sub-wavelength attenuation because they can possess an effective negative bulk modulus and an effective negative dynamic mass density. Bulk modulus is the strain response a material displays under hydrostatic pressure or compression. A negative bulk modulus implies that the material will expand under compression, and then return to its rest volume after compression is removed. This is basically an opposing response to the incident pressure, which causes the attenuation of the incident pressure. Effective dynamic mass density refers to the average force density over the average acceleration a material displays when affected by an impeding force [30]. An effective negative dynamic mass density implies that a force within the material opposes the impeding force, attenuating the transmission of the wave throughout the solid. This phenomenon breaks the limits of the density mass law. This allows attenuation of low frequency waves without increasing static mass or thickness of the material. A material possessing both negative effective bulk modulus and dynamic mass density is therefore optimal for low frequency sound attenuation. These properties, among others, make metamaterials a more efficient choice for MLFN attenuation than phononic crystals [42].

Since metamaterial properties depend on their structure and oscillating frequency of their local resonators, a higher customizability without strict size restrictions can be achieved [23]. In contrast to regular sound attenuating materials, they have no strict size, weight or material composition restrictions. Ideally, a metamaterial designed with the purpose of attenuating MLFN should posses four properties: Extremely low-frequency noise attenuation, high attenuation efficiency, broad attenuation spectrum and surface structure. So far the literature has only been able to achieve this goal partially and so far no metamaterial possessing all these properties has been proposed. This is because achieving one of these properties can deteriorate others. For example, the smaller the desired resonance frequency of a metamaterial is, the bigger the local resonators need to be, which may impede achieving a surface structure [30].

Despite their effectiveness, metamaterials still rely in bulky structures even too big for certain applications. Metasurfaces were thus proposed as an alternative, which are materials with a thinned-out dimension. Metasurfaces were originally proposed for optical waves, but since then, they have been used for acoustic/elastic waves [43]. Metasurfaces show advantages when trying to achieve MLFN attenuation. It is also worth noting that metasurfaces with different resonant frequencies can be stacked, which makes them loose their collapsed direction, but can make them achieve broadband attenuation [30]. The preferred acoustic resonators for noise attenuation are Helmholtz resonators. whichs are hollow structures consisting of both a main chamber and a neck or cavity that connects the inner hollow main chamber with the exterior. The air within the main chamber behaves as a mass with spring constant that acts as a mass spring oscillator under impacting of sound waves [39].
Since metasurfaces are constrained to 2 dimensions, effective attenuation of extremely low frequency waves (0-100 Hz) without sacrificing the small dimensions of local resonators is chalenging. Xinxin et al. [19] analyzed the possibility of enhancing the reflected energy of incoming acoustic waves by using non linearity and second wave harmonics. The metamaterial reflects second harmonic waves which interact destructively with the impacting sound wave. Yong Li et al. [44], designed an acoustic metasurface based on a spiral helmholtz design that can achieve an attenuation coefficient of almost 1 at frequencies as low as 125 Hz with 12.2 mm thickness. This is a subwavelength attenuation ratio of $\frac{1}{223}$.

Current methods of enhancing resonance response include supercell design, multilayer designs, geometrical optimization and resonator coupling. A supercell configuration refers to a periodic structure whose basis is composed of multiple local resonators, each possessing a different resonant frequency. Kexin Zeng et al. [34] designed an extensible hexagonal supercell structure in which the addition of outer layers of resonators causes a broadening of the band gap. In contrast, a multilayer configuration refers to using more than one type of resonator in series or inside other resonators such as in the design by Junzhe Zhu et al. [40]. These designs are able to resonate at their individual resonance peaks without observable dips in their attenuation coefficient while occupying only the volume of the largest resonator.

Geometrical optimization in this case refers to changing the shape of a structure, so that their properties can be tailored to a more desired value. Krupali Donda *et al.* [45] improved the spiral Helmholtz metasurface design, reaching resonant frequencies as low as 50 Hz, with a unit of just 13 mm. This model draws analogy from the way electric circuits operate with electromagnetic waves and current, to achieve an equivalent effect with acoustic waves and air flow. Despite this, the attenuation range of these resonators is quite narrow. Zhiwen *et al.* [46] propose a deep sub-wavelength hexagonal metasurface capable of simultaneous broadband frequency attenuation and crash energy dissipation by mechanical deformation.

Just as geometric optimization is able to lower the resonant frequency of a structure, it can also increase the attenuation coefficient at resonance. Lei Zhang et al. [47] were able to optimize the geometry of the neck of a Helmholtz resonator in order to increase its surface roughness. This in turn increases the amount of energy dispersed by the neck, increasing the attenuation coefficient of the overall resonator, as well as lowering its resonant frequency. Just as optimizing the neck of the Helmholtz resonator can increase its attenuation coefficient, optimizing the geometry of the open cavity is also a viable option. In a study by Yutao Wu et al. [10] they increased the attenuation coefficient of a finger-like structure for a Helmholtz resonator by 5%. The change in geometry consists in uniting the finger-like

section by a common thin chamber or base. This initially shows an increase in resonance frequency as well, but after a certain number of coiled up units are integrated into the structure, the resonance frequency reduces again.

Normally, resonators show a dip in attenuation efficiency at higher frequencies relatively close to their resonant frequency. This phenomenon is termed antiresonance. These dips result in very narrow frequency ranges of sound attenuation as in the case of Helmholtz resonators. Among the most common methods to deal with broadband sound attenuation includes intentional coupling. Resonator coupling refers to the effect a resonator has on adjacent resonators and vice versa, affecting the overall resonance response. A study by D. Roca et al. [48] shows that coupling resonators show promise at eliminating attenuation dips effectively extending the attenuation frequency range. Resonator coupling can be achieved through various methods like changing the dimensions of the resonators or the spacing between them. A study by Liyun Cao et al. [32] analyses the onset of resonator coupling by varying the height of local resonators. This study shows that at a certain frequency-height ratio, resonators are able to couple and sharply increase the overall reflection of the metamaterial. Hongfei et al. [49] proposed the use of non-local coupling effects through the implementation of a structure that mechanically connects non-adjacent resonators, to achieve a broader attenuation frequency range. Coupling can happen in a local or non-local manner. This means that the resonant response of one resonator is influenced by a resonator unit cells away. Just as with local resonator coupling, non-local coupling can help lower the antiresonance response of individual resonators. In the study by Zhiling Zhou et al. [50] they were able to achieve non-local resonance by overdamping (going beyond what is needed to prevent oscillation) a multi-resonant structure. They managed to achieve overdamping by increasing the thickness of the resonators from what is the minimal necessary to achieve perfect attenuation per resonator. This technique to induce non-local resonance was able to extend the attenuation frequency band of the supercell structure. Non-local resonance can also be induced by non-conventional means. Siddhartha Nair et al. [21] proposed a metasurface design consisting of acoustic black holes. Black holes are surface structures, usually concave, that are able to slow down the phase and group velocity of sound waves [31]. The sound waves are deflected, trapped within the acoustic black hole and then dissipated by a viscous structure attached to the resonator. The acoustic black holes in this study had their centers (section of acoustic singularity) directly connected by beams to the rest of the metasurface, in order to induce a non-local resonator coupling. This study was able to lower the overall attenuation frequency range and expand the acoustic band gap of the non-connected structure. Sibo Huang et al. [51] demonstrated that coupling imperfect resonators (resonators with a low absorption peak) can show better attenuation capabilities in a supercell structure, than using quasiperfect individual resonators in the same supercell structure.

So far we have seen that resonator coupling and geometric optimization are fundamental for broadband multi-tonal low frequency sound attenuation. Despite these observations, there is still need for a metastructure able to achieve broadband ultra low frequency attenuation with high efficiency on a metasurface design.

In this thesis a meta-surface is proposed to achieve broadband low frequency attenuation by implementation of geometric optimization by a genetic algorithm, and a common chamber that induces coupling between the local resonators, without sacrificing its surface structure. This metasurface displays coupling phenomena analogue to those of electronic circuits such as frequency pulling and frequency locking which manages to lower the resonance frequency of the local resonators. Through geometrical optimization the structure was able retain a comparable attenuation frequency range width to that of the original metasurface without loss of attenuation efficiency.

2

Background

2.1. Acoustic fundamentals

2.1.1. Sound wave equation

The Navier-Stokes equations are used to describe the state of a fluid medium at any point in time. These equations take into account the conservation of momentum, mass and energy. Supposing a mostly ideal fluid system with no thermoviscous loses, the mass conservation equation (Eq. (2.1)), the momentum conservation equation (also known as the Cauchy equation) (Eq. (2.2)), and the energy equation (Eq. (2.3)) take the respective form:

$$\frac{\partial \rho}{\partial t} + \nabla \cdot (\rho \mathbf{u}) = M, \tag{2.1}$$

$$\frac{\partial \mathbf{u}}{\partial t} + (\mathbf{u} \cdot \nabla)\mathbf{u} = \frac{1}{\rho}\nabla p + \mathbf{F}, \tag{2.2}$$

$$\frac{\partial s}{\partial t} + \nabla \cdot (s\mathbf{u}) = 0, \tag{2.3}$$

where ρ is the fluid density, $\mathbf{u}$ the velocity field, M is the total mass, p is the total pressure, $\mathbf{F}$ is the external force applied to the medium, t is time and s is entropy. Assuming an isentropic process the energy equation can be put in terms of the medium pressure. Merging of the Navier-Stokes equations by substitution of terms gives us the governing wave equation that describes acoustic pressure distribution within a lossless system.

$$\frac{1}{\rho c^2}\frac{\partial^2 p}{\partial t^2} + \nabla \cdot \left(\frac{1}{\rho}(\nabla p - q_d)\right) = Q_m. \tag{2.4}$$

where c is the speed of sound within the medium, $_d$ is the dipole domain source and Q_m is the monopole domain source .Eq. (2.4) is the general wave equation for a pressure sound wave without thermoviscous losses. This equation takes the form of an inhomogeneous Helmholtz equation, assuming zero force sources within the medium. However, if we assume oscillating pressure changes within the material, such as $p(x,t) = p(x)e^{j\omega t}$, and multiplying by ω, the time derivative of the equation reduces to the pressure function:

$$\nabla \cdot \left(\frac{1}{\rho}(\nabla p - q)\right) - \frac{\omega^2 p}{\rho c^2} = Q_m. \tag{2.5}$$

The pressure variable here can be found by solving the eigenvalue problem, taking into account boundary conditions imposed in this case by the geometry of the structure containing the fluid.

This derivation of the pressure wave is only valid for simple geometries. For more complex structures, such as porous materials or narrow structures, thermoviscous losses must be considered. Neglecting these losses can lead to results that significantly diverge from real values (this is further explained in the thermoviscous losses section).

Under the previous assumptions, an incident single-frequency three-dimensional sound pressure wave in air at room temperature and pressure can be described as:

$$\frac{\partial^2 p}{\partial t^2} = -c_0^2 \nabla^2 p. \tag{2.6}$$

where c_0 is the speed of sound in air at room temperature and pressure. Assuming the solution to Eq. (2.6) to be oscillatory and one dimensional (planar), the pressure p has a harmonic form as a general solution. Therefore p can be written as:

$$p = p_0 e^{\mp j\lambda/2\pi(\mathbf{x}-c_0 t)} = p_0 e^{\mp j(k\mathbf{x}-\omega t)}, \tag{2.7}$$

where p_0 is the pressure value at the wave's crest, $k = 2\pi/\lambda$ is the wave number and $\omega = 2\pi c_0/\lambda$ the angular frequency. If we consider a time independent wave, then Eq. (2.7) reduces even further to the form:

$$p = p_0 e^{\mp j(k\mathbf{x})} = p_0. \tag{2.8}$$

It is important to note that $k\mathbf{x}$ is a vector product that possesses magnitude and direction, which describes sound propagation.

2.1.2. Viscous and thermal losses

Part of the energy lost in sound wave transmission is due to thermoviscous losses. Kinetic energy is transformed into thermal energy causing a loss of sound intensity that increases sound attenuation in a structure. This phenomena is specially relevant in surface contact zones, where a boundary layer may form due to an abrupt shift in flow velocity and turbulent flow. Energy dissipation occurs at said surface contact points due to viscous and thermal effects such as viscous shear and thermal expansion. Thermoviscous losses becomes relevant for measuring sound attenuation when dealing with sound transmission within acoustically small regions such as narrow ducts, slits or cavities. Narrow structures experience significant thermoviscous losses due to the increased surface contact between the fluid and the sound-hard surfaces.

The boundary layer is the region within a structure where viscous and thermal losses become important in sound propagation. This region is defined by two key factors: the viscous shear wavelength and the thermal oscillation wavelength. The viscous shear wavelength refers to the wavelength of a shear dissipative wave that displaces particles in a medium. The thermal oscillation wavelength refers to the spatial wavelength of a temperature gradient caused by an oscillation in temperature within the medium. To define a general boundary layer thickness is necessary to use the larger of these two values in order to encompass both phenomena. Beyond these lengths thermoviscous losses become irrelevant. This is because the magnitude of these phenomena decays exponentially beyond these wavelengths (up to 1/500 of the initial amplitude after the first wavelength in fact).

The viscous shear wave and thermal oscillation wavelengths have the respective forms:

$$L_v = 2\pi \sqrt{\frac{\mu}{\pi \rho_0 f}} = 2\pi \delta_v, \tag{2.9}$$

$$L_t = 2\pi \sqrt{\frac{k}{\pi \rho_0 f C_p}} = 2\pi \delta_t, \tag{2.10}$$

where μ is the dynamic viscosity, C_p is pressure constant heat capacity, δ_v is the viscous penetration depth and δ_t are the viscous and thermal penetration depth, respectively. It is to be noted that both

terms depend on the frequency of the wave and their dimensions increase with lower frequencies.

Assuming small harmonic-oscillatory perturbations of the form $x_t = x_0 + x_1 e^{i\omega t}$, where x_0 is the equilibrium position and $x_1 e^{i\omega t}$ is the displacement due to the perturbation, the state variables such as mean flow (u), pressure, density, temperature, external force and monopole domain source take the form $o = o_0 + o_1 e^{i\omega t}$ where o is a place holder variable. Assuming also zero mean flow ($u_0 = 0$) and adiabatic conditions, the goberning equations within the boundary layer become:

$$j\omega\rho + \nabla \cdot (\rho_0 \mathbf{u}) = 0, \tag{2.11}$$

$$j\omega\rho_0\mathbf{u} = \nabla \cdot \left(-p\mathbf{I} + \mu(\nabla\mathbf{u} + (\nabla u)^T) - \left(\frac{2\mu}{3} - \mu_B\right)(\nabla \cdot \mathbf{u})\mathbf{I} \right) + \mathbf{F}, \tag{2.12}$$

$$\rho = \rho_0(\beta_T p - \alpha_p T); T = \frac{\alpha_p T_0}{\rho_0 C_p}, \tag{2.13}$$

where ρ_0 is air density at room temperature and pressure, $\mathbf{I}$ is the intensity vector, μ_B is the bulk viscosity, $_T$ is isothermal compressibility, α_p is the coefficient of thermal expansion, T_0 is the equilibrium temperature and T is the total temperature. When considering the medium as an ideal gas without viscous losses, the state equations can be simplified and merged into the inhomogeneous Helmholtz equation mentioned previously.

2.1.3. Sound transmission and attenuation

Suppose an acoustic wave collides with a flat solid material of a specific thickness. Due to Schnell's Law, the collision generates a reflected and a transmitted sound wave. Each wave has an acoustic energy associated with itself. In Fig. 2.1 we can see how these energies are transmitted during a surface collision.
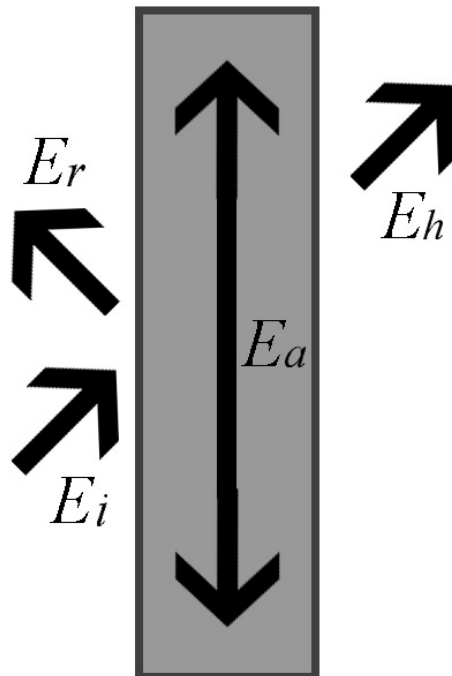
Figure 2.1: Diagram of power transmission of a solid surface. E_i, E_r and E_h are the energies associated with the incident, reflected and transmitted wave respectively. The term E_a refers to the energy dispersed by the material due to thermoviscous losses.

Assuming conservation of energy within the system, the energy of the incident wave is the sum of the energy of the reflected and transmitted wave, plus the energy dispersed by the material itself., i.e.,

$$E_i = E_r + E_a + E_h. \tag{2.14}$$

Each sound wave's acoustic power is measured as:

$$W = \iint_S \frac{p}{2\rho_0 c_0} \cos(\theta) \, \mathrm{d}x \, \mathrm{d}y \,, \tag{2.15}$$

where θ is the angle between the wave vector and the vector normal to the material's surface. The dissipation of energy in the medium results in the loss of some of the incident sound power which is not transmitted to the rest of the waves. Thanks to energy conservation, however, we can measure the power loss dispersed by calculating the ratio between the incident wave power and the transmitted wave power. From this we can calculate what is known as the attenuation coefficient; this coefficient refers to the capability of a material to attenuate incoming energy [8]. The attenuation coefficient is therefore:

$$\alpha = \frac{W_a}{W_i} = 1 - \frac{W_h}{W_i}, \tag{2.16}$$

where W_a, W_i and W_h are the absorbed power and the power associated with the incident and transmitted waves respectively. When $\alpha = 1$ we say the material is a perfect absorber. In the case of acoustic waves this would mean the material attenuates all sound. When the coefficient approaches 0 however, the less effective a material is at attenuating sound. This ratio depends on various parameters such as material composition, dimensions, and particularly the frequency of the colliding wave as well.

The attenuation coefficient is related to the sound reduction index or sound transmission loss (STL), which is often used to quantify the sound absorption performance of a material and is defined as:

$$\mathrm{STL} = 10 \log \frac{1}{h} = 10 \log \frac{W_i}{W_h} = 10 \log \frac{1}{1 - \alpha}, \tag{2.17}$$

where h is the transmission coefficient. This index shows the amount of acoustic power lost by a structure in dB.

2.1.4. Electro-mechanical-acoustic analogy model

Analogy models in science serve to draw similarities between unrelated phenomena. Used as a tool to understand an unknown observation from already known relations. In the case of electro-mechanical-acoustic analogy models, similarities are drawn between the equations describing phenomena such as current flow, resistivity, impedance and so on. One of the first people to research into analogies of this type was Maxwell [52]. It was noted that a mechanical force and velocity of an element had mathematical similarities to that of an applied voltage and electric current. Even more complex mechanical phenomena including the dynamics of a spring or a damper have an electronic analogue. Take for example impedance analogy. Impedance analogy compares mechanical force to voltage induced by inductance, kinetic energy stored within an oscillating spring system to potential energy stored in a capacitor, and mechanical dampened force to a current under electric resistance. Another analogy that allows for description of acoustic or mechanical elements working in parallel or in series is admittance analogy. Admittance analogy in contrast to impedance analogy describes mechanical force as analog to current induced by capacitance, kinetic energy from a spring system to voltage induced by inductance, and a mechanical dampened force to a current induced by voltage under a specific conductance. Table 2.1 displays the mathematical equivalent elements among the previously mentioned analogies.

Analogies between mechanical and electromagnetic phenomena are also present for acoustic phenomena. The description provided on how a local resonator behaves is done using an acoustic-mechanical analogy. Specifically, admittance analogy is very useful for the description of metasurfaces

Mechanical domain		Acoustic domain		Electrical domain			
				Impedance analogy		Capacitance analogy	
Body Acceleration	$\mathbf{F} = m\frac{d\mathbf{u}}{dt}$	Mass	$\mathbf{p} = m\frac{d\mathbf{u}}{dt}$	Inductor	$\mathbf{v} = L\frac{d\mathbf{i}}{dt}$	Capacitor	$\mathbf{i} = C\frac{d\mathbf{v}}{dt}$
Spring	$\frac{d\mathbf{u}}{dt} = C\frac{d\mathbf{F}}{dt}$	Compliance	$\frac{d\mathbf{u}}{dt} = C\frac{d\mathbf{p}}{dt}$	Capacitor	$\frac{d\mathbf{i}}{dt} = C\frac{d\mathbf{v}}{dt}$	Inductor	$\frac{d\mathbf{v}}{dt} = L\frac{d\mathbf{i}}{dt}$
Damper	$\mathbf{F} = R\mathbf{u}$	Resistance	$\mathbf{p} = R\mathbf{u}$	Resistor	$\mathbf{v} = R\mathbf{i}$	Resistor	$\mathbf{i} = G\mathbf{v}$

Table 2.1: Table showing the equivalent mathematical structures on rows for each physics domain where m is mass, $\mathbf{v}$ is voltage, $\mathbf{i}$ is electric current, C is capacitance, L is inductance, R is resistance and G is conductance.

with differently tuned resonators and coupling phenomena between said resonators. These characterizations are mostly done through impedance analysis.

2.1.5. Acoustic Impedance

Electric impedance refers to the opposition a system displays to the flow of an alternating electric current. It is composed by resistance and reactance. Following from the electro-mechanical-acoustic analogy model, we can define acoustic impedance using the impedance analogy. Acoustic impedance is defined as the opposition to the transmission of sound waves through a system. Acoustic impedance is most commonly defined through the ratio:

$$Z = p/Q_v, \tag{2.18}$$

where Q_v is the acoustic volume flow rate. The acoustic volume flow rate refers to the amount of medium displaced by the pressure shift in volumetric terms. The acoustic impedance is a complex number of the form:

$$Z = r + j\chi, \tag{2.19}$$

where r is known as the acoustic resistance and χ is the acoustic reactance.

For analysis of the acoustic impedance of a structure we use the terms specific acoustic impedance and characteristic impedance. Characteristic impedance is the instrinstic opposition of a medium to sound propagation. In case of air at room temperature and pressure, its characteristic impedance is:

$$Z_0 = \rho_0 c_0. \tag{2.20}$$

Specific acoustic impedance is a measurement of the opposition a material or system displays under acoustic interactions. Unlike the characteristic impedance, specific impedance depends on the amount of material and the geometry of the system and it is used to measure the total sound transmission loss. The specific acoustic impedance of a material can be measured with the reflection coefficient (R) of the system as:

$$Z_s = Re\left(Z_s\right) + jIm\left(Z_s\right) = \frac{1+R}{1-R}. \tag{2.21}$$

An acoustic structure such as a resonator at room conditions reaches perfect attenuation when the real part of the specific acoustic impedance is equal to the characteristic impedance of air ($Re(Z_s) = \rho_0 c_0 = Z_0$) and the imaginary part is zero ($Im(Z_s) = 0$) at the same instance [53].

The attenuation coefficient of a material can be measured from the material's specific impedance as:

$$\alpha = 1 - |R|^2 = 1 - \frac{|Z_s \cos\theta - \rho_0 c_0|^2}{|Z_s \cos\theta + \rho_0 c_0|}, \tag{2.22}$$

where $Z_s \cos\theta$ is the effective specific sound impedance at the angle of incidence θ.
Assuming a normal incidence ($\theta = \pi/2$), the specific impedance in Eq. (2.22) changes to:

$$\alpha = 1 - |R|^2 = 1 - \left|\frac{Z_s - \rho_0 c_0}{Z_s + \rho_0 c_0}\right|^2. \tag{2.23}$$

2.1.6. Local Resonance

When a system is in resonance, it absorbs energy from the stimulus and amplifies the response. In local resonance, specific regions of the system respond to an applied stimulus with their own natural frequency of vibration. These regions of the material behave as individual oscillators separate from the matrix or main material and may respond in an in-phase or out-of-phase manner with respect to the stimulus.

The frequency at which both resonance and local resonance are the highest in magnitude is called the resonant frequency. Local resonators can posses a resonant frequency different from the material they are part of, meaning they will have a different response to that of the rest of the material. This can make the material exhibit very particular properties at the resonant frequency of local resonators. Some of such properties are are an effective negative bulk modulus and an effective negative dynamic mass density.

A negative bulk modulus implies that the material will expand under compression, and then return to its rest volume after compression is removed. This is an out-of-phase response to the incident stimuli, which in acoustic metamaterials can aid in the attenuation of the incident pressure. An effective negative dynamic mass density implies that the transmission of a wave through a solid will significantly diminish. This in turn breaks the limits of the Dynamic Mass Law, and allows the attenuation of low frequency waves without increasing their mass or thickness. It is therefore that materials possessing both negative effective bulk modulus and negative dynamic mass density are attractive for low frequency sound attenuation.

Among the types of acoustic resonators that have been of interest in literature are acoustic black hole resonators, Mie resonators, and Helmholtz resonators. Acoustic black holes consist of a concave structure, usually circular in shape, that is able to change the wave vector of a sound wave and change its transmission path, trapping it within a resonator analogue to light and black holes. Mie resonators are maze like open structures with sound rigid walls that show Mie resonance with acoustic waves, analogue to Mie resonance in photonics. Helmholtz resonators consist of an open cavity filled with air, and a neck or tube that connects the inner cavity with the outside.

2.1.7. Resonator coupling

Resonator coupling is the phenomenon in which the resonant response of one resonator alters the resonant response of an adjacent resonator. Coupling can happen both in a constructive or destructive manner, meaning it can enhance or reduce the intensity of the resonant response of the resonators. Various factors affect coupling such as the relative position of each resonator, the orientation of oscillation, and the proximity of their own resonant frequency, all with respect to each other. Junzhe et al. [40] developed a Helmholtz multilayer structure consisting of multiple Helmholtz resonators stacked inside each other. The coupling effect between the neck of resonators was shown to depend on their position with respect to the closest neighbouring necks. This indicates that proximity to adjacent resonators can influence their own resonant response.

Resonator coupling is the basis of supercell research. Supercell metamaterials are periodic structures whose unitary base structure is composed of multiple local resonators, each tuned to a different frequency. Local resonators respond to a specific frequency and quickly lower their response for different frequencies. The purpose of a supercell is to add up the individual responses of each resonator so no "response gap" are observable. This base structure is therefore designed to display a frequency broadband response.

Proper coupling is important to achieve broadband response, since improper attenuation can hinder the response of the overall structure. Proper coupling can help to not only avoid diminishing the resonator's response, but to also enhance it. Sibo et al. [54] performed a study on the effects of coherent coupling of "weak resonances" and showed that under coupling, the individual response of each resonator could be enhanced. Roca et al. [48] proposed the use of coupled resonators to extend the working acoustic attenuation bandgap of a metamaterial to lower frequencies. This was done using mul-

tiple local resonators with different working frequencies to give a more continuous attenuation bandwith when compared to uncoupled multi-resonator metamaterials.

Resonator coupling is also seen in electronic systems. Thanks to the electro-mechanical-acoustic analogy we can apply methods to characterize coupling between electric resonators to acoustic resonators. In electronic systems coupling between resonators can be calculated by comparing their scattering parameters. In the acoustic realm some of these scattering parameters are the equivalent to the reflection and transmission coefficient. Some of the phenomena observed within electronic resonator coupling is the downshift and merging of resonance frequencies. Both phenomena are known as frequency pulling and frequency locking, respectively [55].

Another way to characterize coupling derived from the electro-mechanical-acoustic analogy model is to measure the impedance of a system with two or more impedance elements in parallel/series. The total acoustic impedance of n acoustic attenuating structures connected in parallel can be measured through:

$$\frac{1}{Z} = \sum_{i=1}^{n} \frac{1}{Z_i},\tag{2.24}$$

where Z_i is the acoustic impedance of each individual structure. This is in the case of uncoupled resonant structures. In the case such resonators have a degree of coupling, the total acoustic impedance will change. Therefore we can measure the degree of coupling between resonators by measuring the difference between the predicted reflection/attenuation coefficient to the actual reflection/attenuation coefficient of the coupled system.

2.2. Geometric optimization

By geometric optimization we mean the use of numerical methods to vary structural parameters in order to minimize or maximize an objective function. This is fundamental to achieve maximum efficiency in local resonator structures.

One of the methods for geometric optimization is genetic algorithms. These are optimization methods inspired in biological evolution. It takes a sample population of individuals that encode the parameters of the problem to produce an off-spring population, whose properties are based on those of their parents. The parents that are chosen to make the offspring are chosen through selection methods by fitness, truncation, tournament, etc. Offspring properties are obtained through mutation (slight random change in their parents' properties) and through a crossover (combination of the parents' properties). From this point, the best fit parameters of the offspring that approach the goal of the optimization, called the elite, are chosen to be the parents of the next generation. This process repeats until one of the stop criteria of the algorithm is reached. Some of the stop criteria can be a threshold value (whenever the objective function reaches said value the optimizations stops), a limit to the number of generations or time, when the value of fitness function stops changing considerably around the best point, and so on.

2.3. Helmholtz resonator

Helmholtz resonators were first introduced by Helmholtz himself in 1862 on his book "On the sensations of tone as a physiological basis for the theory of music". They are usually used for passive noise attenuation in structures without solid material obstruction, such as in the case of pipes and air ducts [36].Particularly, Helmholtz resonators have been of interest in research since they display both negative effective bulk modulus and negative dynamic mass density. They are of simple design and do not depend on material composition as long as the materials can be considered sound rigid. Despite their narrow attenuation capacity, Helmholtz resonators have been shown to poses a high attenuation coefficient, particularly at low frequencies. Also their band narrowness has been shown to be easily compensated by the use of multiple resonators tuned at different frequencies [37]. And finally, they do

not have a strict geometric shape, which allows for design exploration. In fact, the Helmholtz resonator geometry has a considerable effect on its resonance response, even when controlling for absolute volume, neck cross sectional area and length. The fact that Helmholtz resonators do not have a preset geometric design is of great interest to design metasurfaces.

The mechanism of work of a Helmholtz resonator is as follows: Whenever a pressure wave of resonant frequency comes in contact with the neck opening of a Helmholtz resonator, air flows into the neck increasing the air pressure inside the resonator's cavity. In response to this increase in pressure, the air compresses increasing its density. Since the air outside the resonator at this point possesses a lower air density compared to that within the resonator, the air within the resonator expands in response. The expansion of the air within the cavity causes the air inside the cavity to exit through the neck in opposition to the incoming air flow. After the air exits the resonator, the air density within the resonator lowers below the air pressure outside the cavity, causing air to flow back in. Fig. 2.2 displays the aforementioned process in three stages.
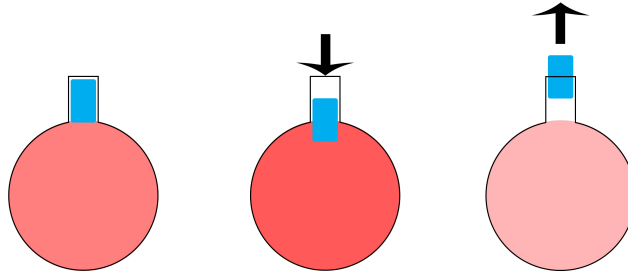
Figure 2.2: Displacement of the acoustic mass in the neck (blue) of a Helmholtz resonator under acoustic wave pressure at resonance frequency. The intensity of the red color within the cavity of the resonator represents the air mass density, while the black arrow represents the displacement vector of the acoustic mass of the neck.

Following the mechanical-acoustic model analogy, the acoustics of a Helmholtz resonator can be described as a dampened mass oscillator in function of its geometry and the physical intrinsic properties or air (under isothermal conditions). Such analogy can be seen in Fig. 2.3. From this analogy we can calculate the resonance frequency. The equation of motion of the Helmholtz resonator mechanical analog is:

$$m\ddot{x}(t) + c_d\dot{x}(t) + kx(t) = f(t), \tag{2.25}$$

where m is the acoustic mass of the neck of the resonator (which takes the roll of the mass displaced by the spring under the analogy), c_d is the linear viscous damping coefficient, and k is the linear elastic stiffness. These properties are the mechanical analogues to thermoviscous losses and acoustic stiffness respectively.

Under the induction analogy, a Helmholtz resonator can be treated as a electronic structure, consisting of an inductance, a capacitor, and an electric impedance element (if dampening or energy losses
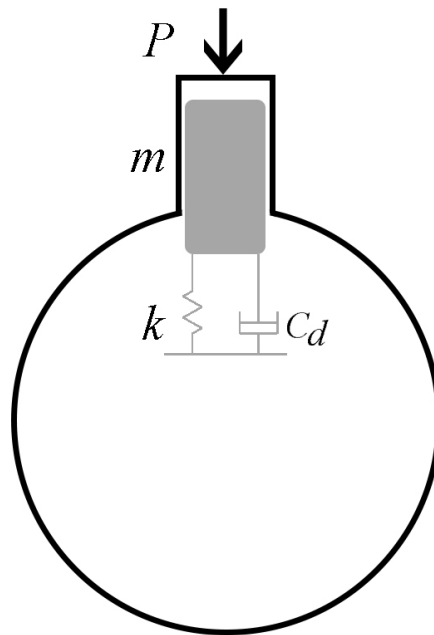
Figure 2.3: Spherical Helmholtz resonator and its mechanical analog (in gray) that describes the movement of the acoustic mass. P represent the incoming pressure, m is the acoustical mass of the neck, k is the equivalent spring constant and c_d is the equivalent dampening factor.

are considered) all in a series arrangement as displayed in Fig. 2.4.
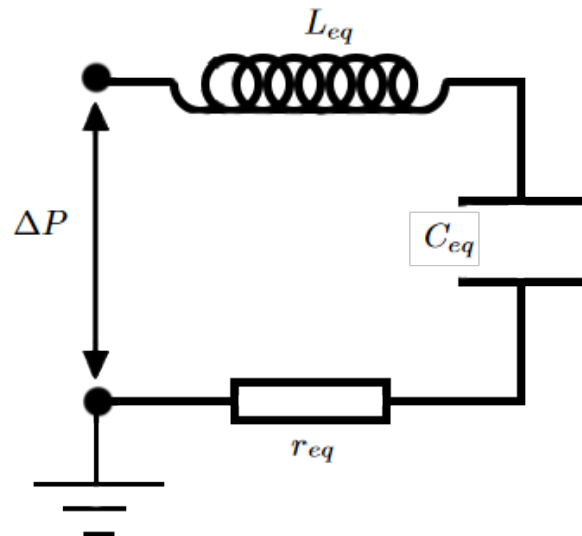
Figure 2.4: Sketch of the electronic equivalent of a Helmholtz resonator under induction analogy. ΔP is the potential diference, L_{eq} is the equivalent inductance, C_{eq} is the equivalent capacitance, and r_{eq} is the equivalent resistance.

The electronic equivalent values for the capacitance, inductance, and impedance of the components in the Helhmoltz resonator circuit are characterized by the geometric and medium properties as:

$$L_{eq} = \frac{\rho l_{eff}}{S} = m, \tag{2.26}$$

$$C_{eq} = \frac{V}{\rho c^2}, \tag{2.27}$$

$$Z_{eq} = r_{eq} + i\chi_{eq} = \frac{8\pi\mu l}{S} + j\left(\omega L_{eq} + \frac{1}{\omega C_{eq}}\right), \tag{2.28}$$

where L_{eq} is the equivalent inductance, C_{eq} is the equivalent capacitance, Z_{eq} sis the equivalent impedance, r_{eq} is the equivalent resistance, χ_{eq} is the equivalent reactance, l_e is the efficient length of the neck ($l_e = l + 2\delta$) where l is the actual length of the neck (and δ is a correction factor), V is the air volume inside of the cavity and S is the surface area of the neck at its exterior face, and μ is the dynamic viscosity of air. Do notice that the acoustic reactance (χ_{eq}) directly depends on the inductance and capacitance. From this deduction, we can actually deduce the resonance frequency by minimizing Z_{eq} in function of ω. Z_{eq} will arrive at a minimum value when the reactance reaches zero or a minimum value. Clearing for ω and substituting the mass and capacitance within the equation, we can arrive at the expression for the resonant frequency in terms of the geometrical parameters of the resonator:

$$f = \frac{c_0}{2\pi}\sqrt{\frac{S}{Vl_e}}. \tag{2.29}$$

For subwavelength acoustic resonators such as Helmholtz resonators, it becomes important to consider thermoviscous losses. The neck of the Helmholtz resonator itself is responsible for a significant amount of energy dispersion during resonance, which is why its dimension is highly relevant when it comes to its own attenuation capacity [10]. Viscous effects of the boundary layer within the neck of the Helmholtz resonator are responsible for rapid sound attenuation, as energy is lost due to friction between the airflow layer and the walls of the resonator's neck [40]. When frequencies between incoming air waves and the Helmholtz resonator's own resonance frequency become congruent, air flow within the resonator raises significantly. Therefore air friction within the resonator, especially in the neck, becomes substantial. Here most of the sound wave energy is therefore transformed into heat, which disperses sound and attenuates sound intensity [40].

3

Methodology, Results and Analysis

3.1. Simulation parameters

The models were built in COMSOL according to the supplementary material provided by Kexin et al. [34] for the experimental model.

The software built-in material properties of air at room temperature and pressure were used. The values were respectively, $c_0 = 343 \text{m s}$, $\rho_0 = 1.2 \text{kg m}^{-3}$ and $Z_0 = c_0\rho_0 = 411.6 \text{kg m}^{-2}\text{s}^{-1}$. Both the pressure acoustics module and thermoviscous model were used, as well a module that describes the interaction between both domains. Both modules solve for the linearized Navier Stokes equations in order to describe the propagation of pressure waves within both sections.

An incident sound pressure wave of 1Pa of magnitude and varying frequency was utilized as the incident sound wave within the simulated impedance tube. No initial phase shift was considered for the incident wave. The incident pressure plane wave equation used in the COMSOL simulation is of the form

$$P_i = P_0 e^{\phi} e^{-ik_s \frac{(xe_k)}{|e_k|}},$$ (3.1)

where P_0 is the initial wave amplitude, ϕ is the wave phase, e_k is the dimensionless wave direction, and $k_s^2 = (\frac{\omega}{c_0})^2$ is the complex wave number [56]. Replacing the definition of k_s in Eq. (3.1) makes the pressure wave equation a function of ω, therefore $P(\omega)$. The incident pressure wave equation is derived from both Euler's equation and the continuity equation [56].

It is to be noted that the waveguide has an equivalent electronic element whose impedance and capacitance are measured as:

$$L = \rho_0 l_w / 2D^2,$$ (3.2a)

$$C = D^2 l_w / 2\rho_0 c_0,$$ (3.2b)

where D is the side length of the waveguide (assuming a square waveguide) and l_w is the length of the waveguide in the direction of the incident pressure wave vector. Under this analogy resonators have an added acoustic resistance term r, unlike the waveguide, to take into account thermoviscous losses due to their small size; i.e., it is assumed the waveguide is a big enough structure so that thermoviscous losses are negligible within most of this region. The thermoviscous model was used on the metasurface domain, as well as on a section of the impedance tube domain, specifically the section closest to the metasurface. The thickness of the section of the impedance tube in which we will use the thermoviscous acoustics model is determined by the thermal and viscous boundary layer at the lowest simulated sound frequency. Specifically we take the largest of the values so that both thermal and viscous effects are taken into account properly. The remaining section of the impedance tube is considered smooth, big and far apart enough from the metasurface to ignore thermoviscous effects.

Here the pressure acoustics module was used to save computation time.

The transfer function describes the transmission of energy from one point to the other. In the case of an impedance tube, these points would be microphones as shown in Fig. 3.1.
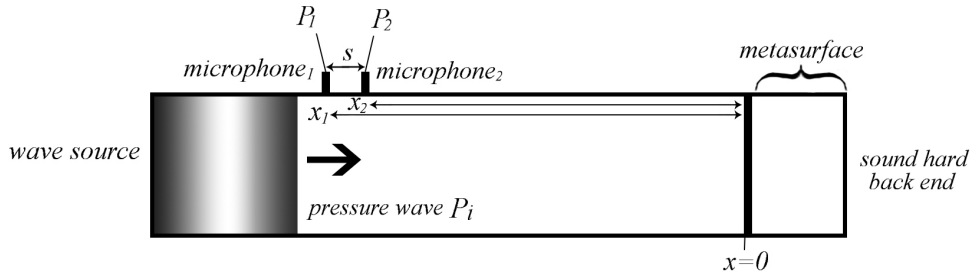
Figure 3.1: Experimental setup of an impedance tube for sound attenuation measurement. P_i is the incident pressure wave, P_1 and P_2 are the measured pressure intensities at the microphones 1 and 2, respectively, s is the distance between the microphones, and x_1 and x_2 are the distances between the metasurface and microphones 1 and 2, respectively.

The pressure as a function of frequency is measured in each microphone. From this measurements, the transmission function is

$$H_{12} = \frac{P_1(\omega)}{P_2(\omega)}, \tag{3.3}$$

where $P_1(\omega)$ and $P_2(\omega)$ are the acoustic pressure measured at the microphones 1 and 2, respectively. From this value, the acoustic reflection factor can be obtained as

$$R = \frac{H_{12} - e^{-jks}}{e^{jks} - H_{12}} e^{2jk(s+x_2)}, \tag{3.4}$$

where s is the distance between both measuring microphones, x_2 is the distance between microphone 2 to the metasurface. From R we can obtain the values for the sound attenuation coefficient and the sound transmission values. Likewise, from here we can obtain the values for the specific acoustic impedance from Eq. (2.21).

3.2. Chamber analysis

A simulation was done to analyze the effects of an added chamber has on a two Helmholtz resonator structure, where both resonators are tuned to different resonance frequencies. Fig. 3.2 displays a two resonator system with and without a connecting chamber, respectively. The model utilized to analyze the coupling of Helmholtz resonators is the inductance analogy model. Under this analogy, two Helmholtz resonators connected to a waveguide such as an impedance tube possess an electronic analogue as displayed in Fig. 3.3. Assuming a planar acoustic wave with normal incidence, both resonators are connected in parallel to the waveguide because they interact with the same acoustic pressure value. For metasurfaces with more than 2 resonators, it is just a matter of adding the equivalent circuits for each additional resonator, all connected in parallel at the same node.
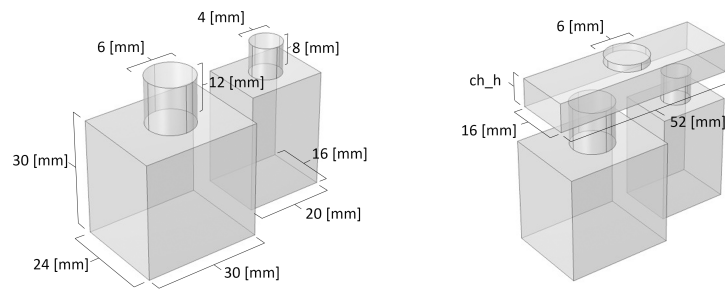
Figure 3.2: Two Helmholtz resonator base unit dimensions with a connecting chamber (right) and without a chamber (left). Both resonators have a height of 30 mm. The chamber depth (ch_h) varies during the experiment.
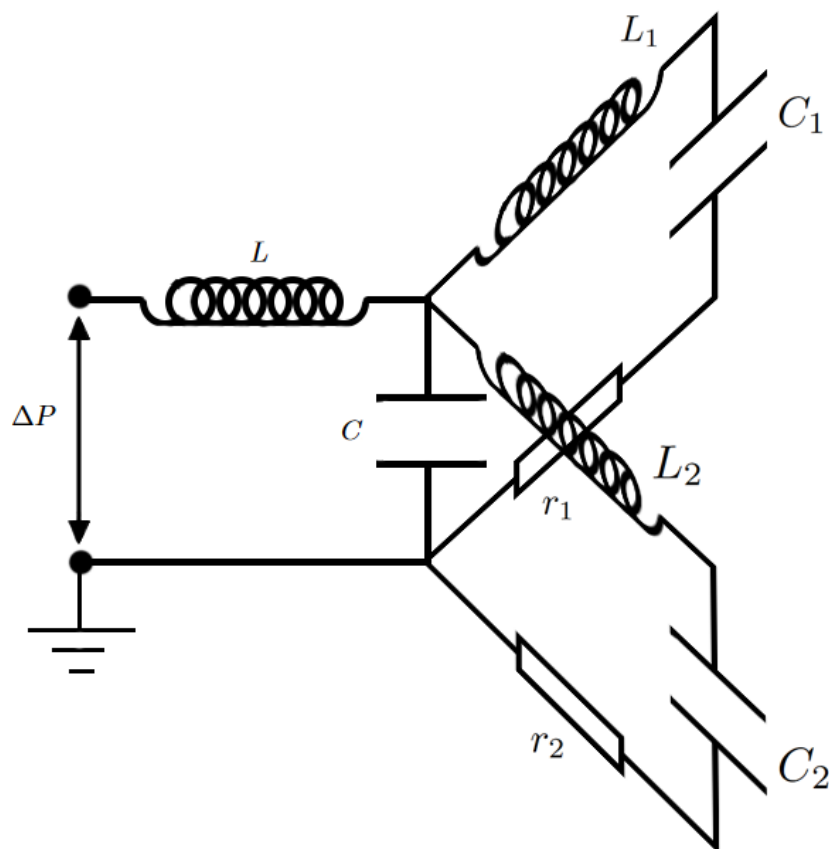
Figure 3.3: Electronic structure of an impedance tube with two resonators connected in parallel. L and C are the corresponding inductance and capacitance of the wave guide and L_i, C_i, and r_i are the impedance, capacitance and resistance elements associated with the i Helmholtz resonator.

Fig. 3.4a, 3.4b and 3.4c show results on chamber depth and its influence on the acoustical properties of a two resonator Helmholtz structure as displayed in Fig. 3.2. It is noticeable that just the presence of a connecting chamber decreases the resonance frequency of both resonators, while also pulling both closer to each other. The downshift in resonance frequency is a phenomena arising from coupling, called frequency pulling. This phenomenon happens when two or more resonators shift their resonance frequency due to their interaction with nearby resonators. We can also observe that the difference between both resonance frequencies diminishes. This is known as frequency locking. Multiple

(a)

(b)

(c)
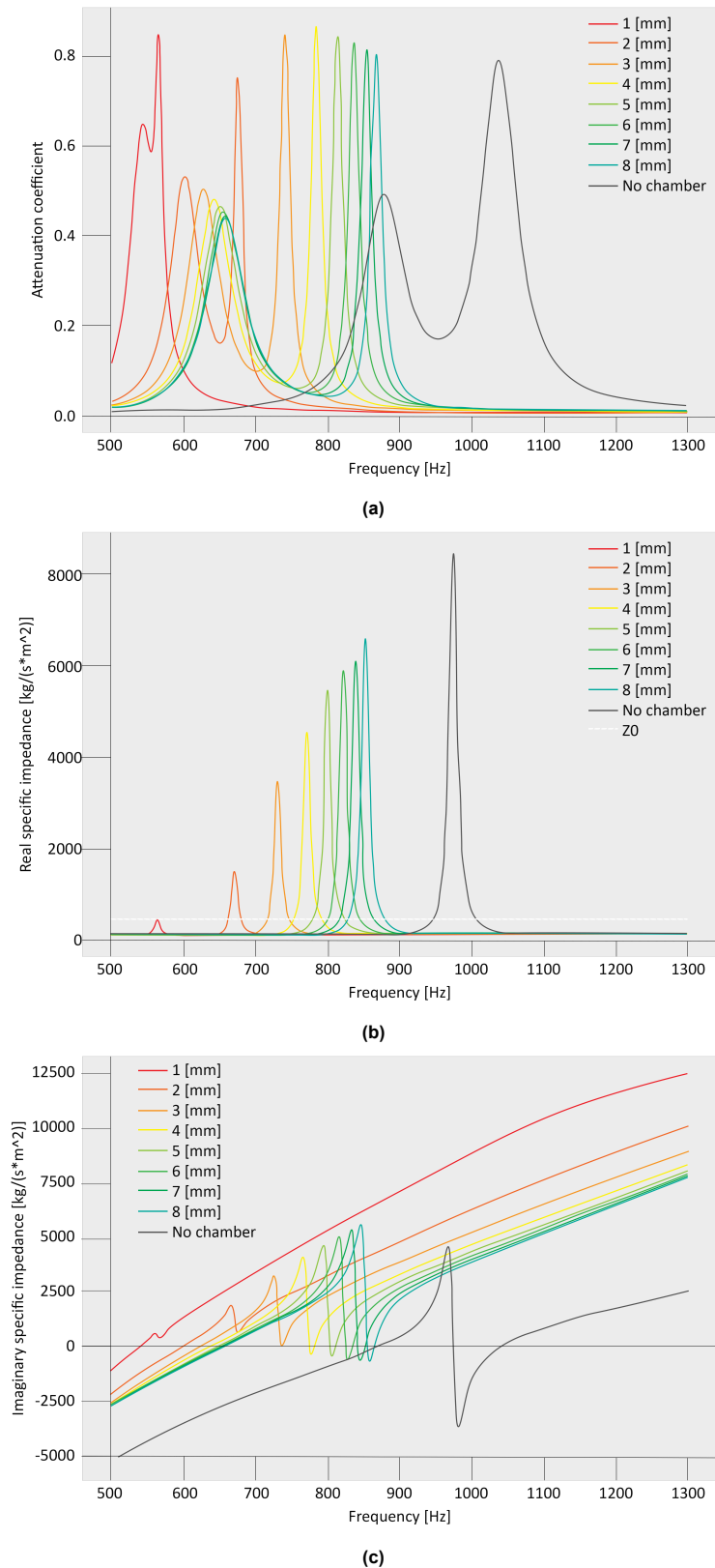
Figure 3.4: Attenuation coefficient (3.4a), real impedance (3.4b), and imaginary impedance (3.4c) of the two Helmholtz resonator system with a common chamber from Fig. 3.2. The numbers in the legends of each figure display the different depths of the connecting chamber in mm. The $Z0$ line displays the characteristic impedance of air and the line that says "No chamber" in the legend of each figure displays the case in which the metasurface structure has no added chamber.

resonators enter in resonance simultaneously at the same frequency, merging neighbouring frequencies. This is indicative of a higher coupling strength between resonators. Frequency pulling and locking are concepts originally used for electronic resonators, but they can be applied to acoustics thanks to the electro-mechanical-acoustic analogy model. This coupling causes a change in the effective capacitance and effective inductance of individual LC resonators.

The attenuation coefficient of the structures with a chamber mostly reach higher efficiency than the structures without a chamber. If we take a look at the real and imaginary values of the impedance in both cases, we can see that the real impedance of the structure without a chamber is way higher than that of the chambered structure. However the imaginary impedance of the chambered structures is generally larger than that of the one without a chamber. In fact, the smaller the chamber, the higher the imaginary impedance of the overall structure. This pinpoints that with a decreasing chamber size, the acoustic attenuation depends less on thermoviscous effects and more on the equivalent inductance and capacitance terms. This therefore suggests that the addition of a chamber structure can also lower the resonance frequency of a multiple resonator structure without sacrificing efficiency or surface depth.

3.3. Geometric optimization

Zhiwen et al. [46] were able to design a hexagonal metasurface structure composed of Helmholtz resonators capable of broadband attenuation in the 300-600 Hz range, as well as high load-bearing strength against compression. We decided to use this design because hexagonal designs are most optimal for both compact packing of resonators as well as for mechanical stress and energy dissipation [46]. We performed a geometric optimization on this design to attempt to increase the overall sound reduction within its intended frequency range of 300-600 Hz.

We used parallel computing to do the optimization. Parallel computing involves performing multiple calculations at the same time. Certain optimization calculations can be done simultaneously, reducing the total computation time. We used a genetic algorithm. A genetic algorithm is a computational method inspired by natural evolution. A parent set of data produces various data sets. The fitness of these data sets is evaluated and the fittest of these sets survives. A genetic algorithm consists of both a genetic representation of the data used in the algorithm and a fitness function that the data is evaluated against. The fitness function uses the population data to obtain a value, which is considered the "fitness" of the population itself. The offspring data goes through crossover and/or mutation in order to produce candidates for the next generation of data. Crossover refers to the combining of parent data sets' properties to produce the next generation's properties, and mutation refers to a random shift in the subsequent generation properties independent of the parent's properties. Our algorithm uses both methods to produce the next generation candidates. These potential candidates are evaluated by the fitness function. From these data points, the fittest data set will make up the next generation of parent data. This process repeats until a stop criterion is met. The optimization can have many different stop criteria, like achieving a certain level of fitness, reaching an error threshold, reaching a maximum computation time, or reaching a maximum number of generations. The process can be seen visually in Fig.3.5

The parameters subject to our genetic optimization were the length and diameter of each resonator's neck, as well as the inner resonator's side length. Only the outer resonators side length and surface depth were kept constant to maintain metasurface unit cell volume. The fitness function used during optimization was

$$A = \Sigma_{i=0}^{n}\alpha(\omega_i), \tag{3.5}$$

where ω_i are the frequency values at which the attenuation coefficient was measured within the frequency range of interest. This was done to achieve the highest attenuation coefficient possible. Each ω_i value is 0.25 Hz apart from the previous and/or later frequency. Our stop criteria was a maximum set number of 20 generations.

The geometry of the structure before optimization as designed by Zhiwen et al. is displayed in
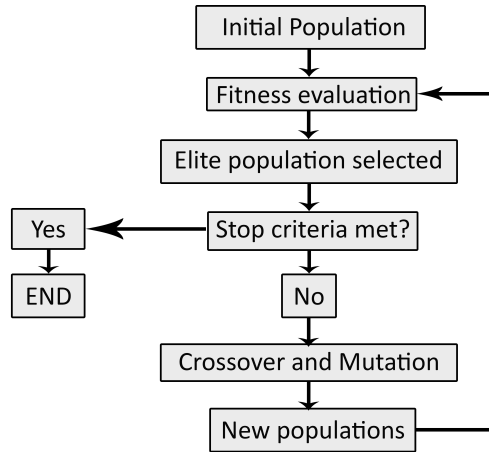
Figure 3.5: Flow chart of a genetic algorithm.

Fig. 3.6a, with its respective parameter values and average attenuation coefficient within the 300-600 Hz sound range in Table 3.1. The geometry parameter values and average sound attenuation of the structure after optimization are displayed in Fig. 3.6b and Table 3.1, respectively. The attenuation spectrum of the geometries before and after optimizations are displayed in Fig. 3.7a and Fig. 3.7b, respectively.

We can observe in the optimized structure Fig. 3.6b that the inner resonator is substantially reduced in size while prioritizing the outer resonator's volume. Despite this reduction in volume, the number of peaks in the attenuation coefficient spectrum remains the same, and the average attenuation coefficient increases by 0.06. While this increase is not substantial, the geometric optimization could potentially aid in creating an equally efficient structure with different geometry. To analyze the attenuation bandwidth, we can measure a quantity known as the half absorption bandwidth (HABW), which refers to the frequency range where the attenuation coefficient is continuously greater than 0.5. In Table 3.1, we can observe that the HABW increases by 35% after optimization, despite the average attenuation coefficient not showing a significant increase. Due to the increase in bandwidth we proceeded to use the optimization technique to incorporate a common chamber into the structure, in order to examine the potential benefits of this addition.

3.4. Chamber and optimization analysis

A geometric optimization was performed using Matlab utilizing parallel computing and the genetic algorithm in the previous section. First, the unit cell of the metasurface was optimized by maximizing the integral of the attenuation coefficient over the frequency range of interest (300-600 Hz). Two models were optimized: One without an added chamber, and one with an added chamber, as seen in Figs. 3.8a and 3.8b, respectively. All necks were optimized individually. Each had their diameter and length changed. The diameter of the neck was constrained to remain smaller than the width of its respective resonator (taking into account wall thickness). The length of the neck was also changed while maintaining the neck smaller than the length of the resonator plus the wall thickness. The length of the outermost resonators is kept constant in order to keep the surface density of the resonators within the metamaterial constant. We set the height of the metasurface constant to maintain metasurface thickness.

To analyze the total sound loss within a specific frequency range, we define the value cumulative attenuation response (CAR). We define this value as the integration of the attenuation coefficient over a frequency range. In this case, the CAR was measured using the trapezoidal rule. We can observe in Tables 3.2 and 3.3 that the CAR of the structures in Fig. 3.8a and 3.8b shows a larger increase
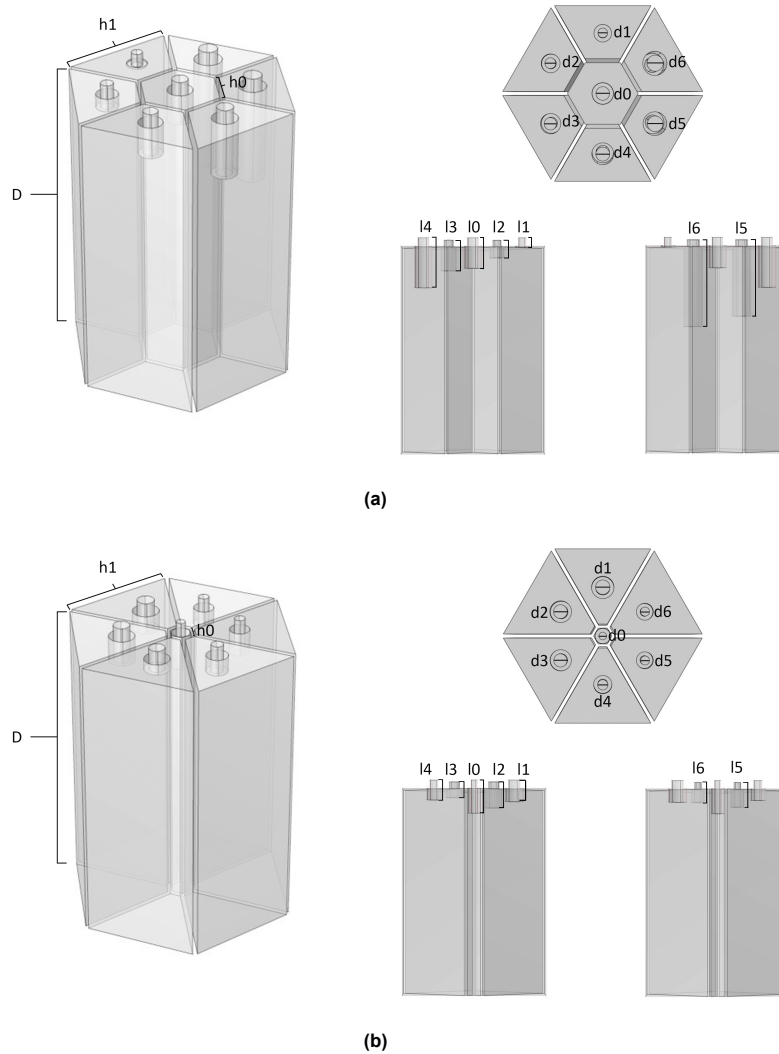
Figure 3.6: Hexagonal Helmholtz metasurface base structure by Kexin et al. [34] before parameter optimization (3.6a) and after optimization (3.6b). The respective optimized parameters are the side length of the inner resonator (h_0), neck diameter (d_i) ,and neck length (l_i) of each i resonator. The total metasurface depth (D) and outer resonator side length (h_1) were kept constant to maintain the total volume of the base unit constant.

in comparison to the optimization in Table 3.1. This suggests that the geometric optimization is a reliable method to improve the acoustics of the structures in an automated way without much human supervision. The HABW of Figs. 3.8a and 3.8b also shows a significant improvement, increasing by 15% and 35%, respectively, despite the optimization not directly targeting bandwidth.

The optimization of the model with the added chamber was similar to the previous model, with a few exceptions. The total depth of the metasurface was now defined by the surface wall thickness and the resonator depth, as well as the depth of the chamber. Previously, the metasurface's unit cell depth equaled the resonator depth plus the surface wall thickness, but in this model, the same total depth was maintained while also accounting for the chamber depth. This was done to properly compare the efficiency of both structures with the same metasurface thickness.

Both Fig. 3.9c and 3.9d display the simulated attenuation coefficient curves of the most optimal parameter values to maximize the attenuation coefficient over the range of 300-600 Hz. Both optimizations were set with a population of 250 and were set to run for 20 generations. Smaller population/generation settings would reduce the quality of the final results and bigger population/generation settings would increase computation time, to the point where the optimizations would become unfeasible for this project. The final values of the optimization parameters are in the tables 3.4 and 3.5. The optimized geometries

Parameter	Structure before optimization Value [mm]	Structure after optimization Value [mm]
D	50	50
h1	20.02	20.02
h0	7	1.8372
d0	2.7	1.5202
l0	7.3	7.9966
d1	1.9	2.8845
l1	2.3	5.2038
d2	2.15	2.7449
l2	4.3	6.3781
d3	2.45	2.6494
l3	7.5	3.8087
d4	2.75	2.0529
l4	12	4.8045
d5	3.1	1.7830
l5	18.8	6.0595
d6	3.2	1.7897
l6	21.4	4.8913
Attenuation coeff.	Average	Average
	0.62	0.68
HABW	Range [Hz]	Range [Hz]
	(345 - 530)	(310 - 560)

Table 3.1: Parameter values, average sound attenuation coefficient, and half attenuation bandwith (HABW) within the 300-600 Hz frequency range of both Fig. 3.6a and 3.6b.
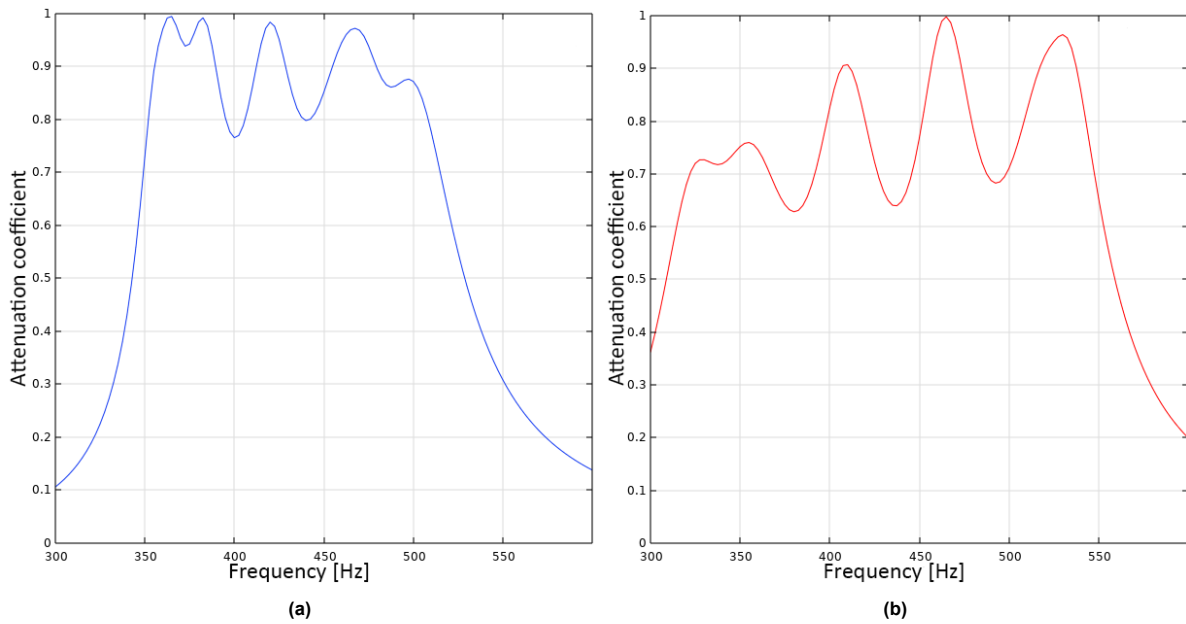
Figure 3.7: Attenuation coefficient spectrum in the 300-600 Hz frequency range for Fig. 3.6a (a) and Fig. 3.6b (b).

Values	Before Optimization	After Optimization
Cumulative attenuation response	174.15	191.23
HABW range	(367.5 - 587.5)	(345 - 600)

Table 3.2: Value comparison between the hexagonal structures without a chamber before optimization (Fig 3.8a) and after optimization (Fig 3.9a).

(a) **(b)**
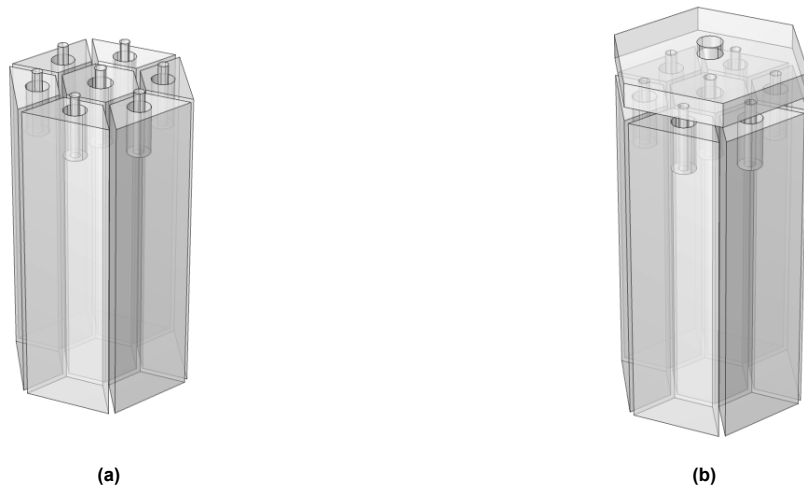
Figure 3.8: Hexagonal Helmholtz metasurface without a chamber (Fig. 3.8a) and with a chamber (Fig. 3.8b) before optimization following the design from Kexin et al. [34].

(a) **(b)**

(c) **(d)**
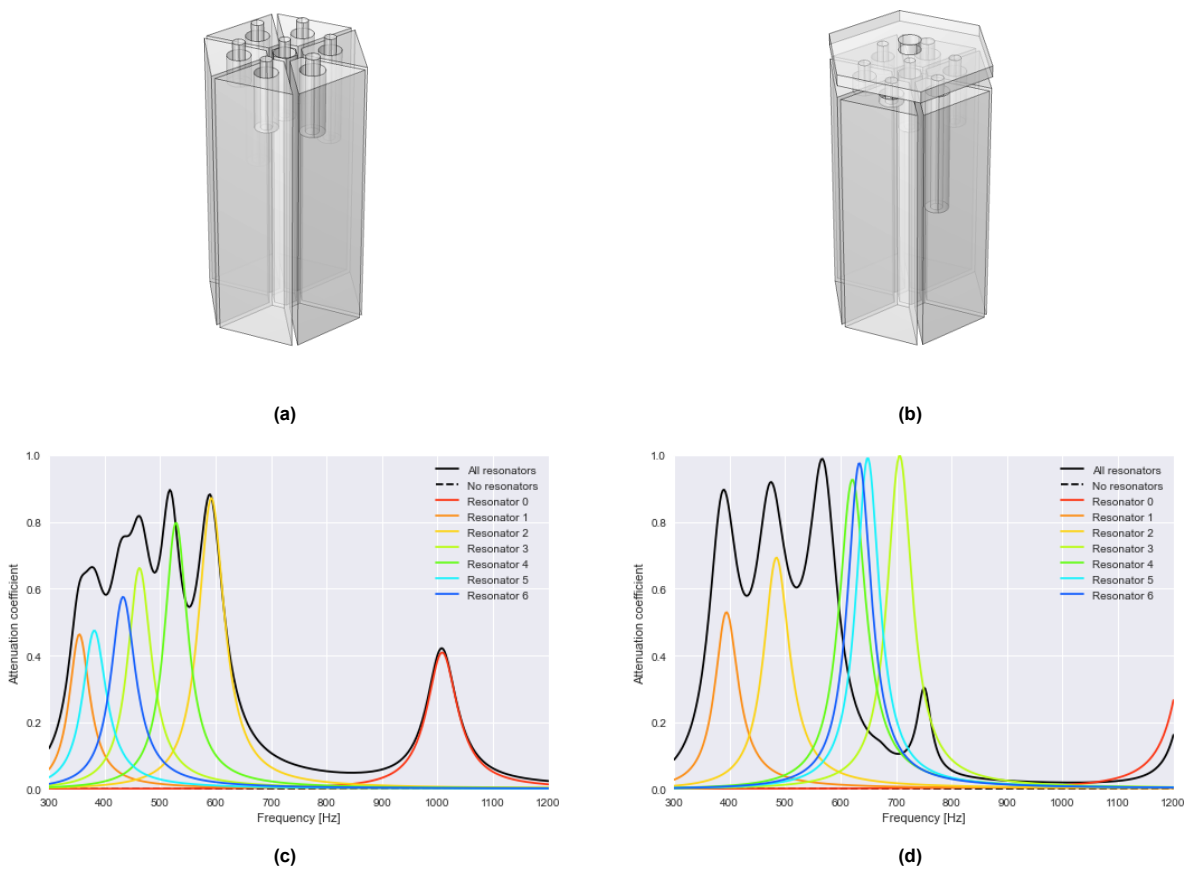
Figure 3.9: Final optimized hexagonal structure without a chamber (Fig. 3.9a) and with an added chamber (Fig. 3.9b), with their respective attenuation coefficient curves (Fig. 3.9c and 3.9d). The structures were optimized to maximize attenuation coefficient in the 300-600 Hz range. The curves illustrate the individual attenuation coefficient of each resonator, as well as the attenuation coefficient of the overall base unit. The dashed line showing the attenuation of the base unit without any resonators was to demonstrate that the chamber does not attenuate sound independently within the selected frequency range.

are shown in Fig. 3.9a and 3.9b

The first curve in Figs. 3.9c and 3.9d with the label "All resonators", represents the overall attenuation spectrum of the full structures, from 300-1200 Hz. This extended range was used due to the
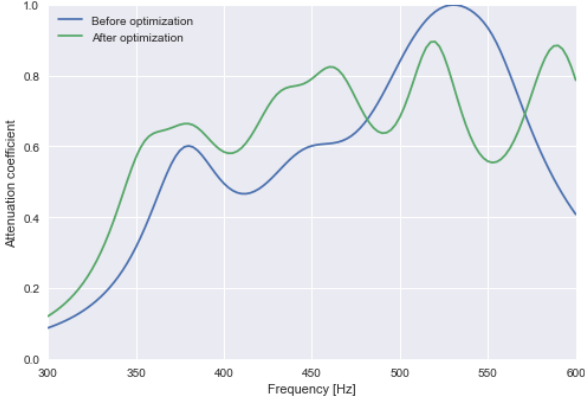
Figure 3.10: Attenuation coefficient curves for the hexagonal structure without a chamber before optimization (Fig 3.8a) and after optimization (Fig 3.9a).
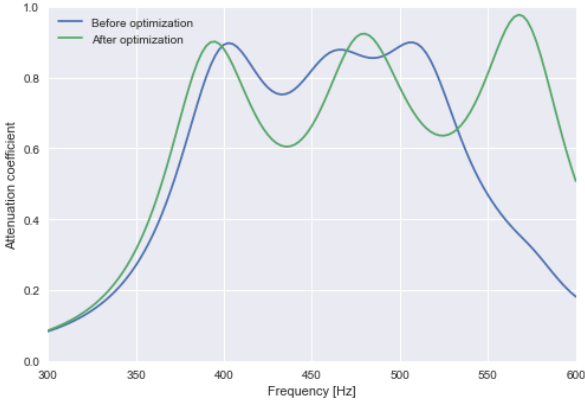
Figure 3.11: Attenuation coefficient curves for the chambered hexagonal structure before optimization (Fig 3.8b) and after optimization (Fig 3.9b).

Values	Before Optimization	After Optimization
Cumulative attenuation response	172.56	193.19
HABW range	(372.5 - 547.5)	(362.5 - 600)

Table 3.3: Value comparison between the chambered structure before optimization (Fig 3.8b) and after optimization (Fig 3.9b).

appearance of individual resonance frequencies at higher values than in the optimization range. The remaining curves marked by the Resonator x label show the attenuation spectrum of each individual Helmholtz resonator within the hexagonal structure, where all other resonators have been removed. This was done to gain insight into the contribution and frequency shift of each resonator under the presence of the remaining resonators within the metasurface.

Resonator	Neck length [mm]	Neck diameter [mm]
0	11.6734	1.5245
1	21.7427	1.7617
2	6.0060	1.7089
3	10.2933	1.6651
4	11.3339	1.9567
5	15.6334	1.6401
6	12.1339	1.6597

Table 3.4: Optimized dimensional parameters of the metasurface without a chamber as displayed in Fig. 3.9c. The side length of the hexagonal inner resonator (resonator 0) was also optimized. Its value is 1.8415 mm

Resonator	Neck length [mm]	Neck diameter [mm]
0	10.3225	1.5195
1	3.9404	1.5518
2	4.1814	1.6272
3	3.1637	1.7289
4	20.2290	1.7419
5	9.9003	1.6636
6	4.1363	2.0126

Table 3.5: Optimized dimensional parameters of the metasurface with an added chamber as displayed in Fig. 3.9d. The side length of the hexagonal inner resonator (resonator 0), as well as the chamber depth and orifice radius were also optimized. Their values are 1.8214 [mm], 1.6343 [mm] and 1.5565 [mm] respectively.

Metasurface	Attenuation percentage [%]	Neck's average volume [mm^3]
No Chamber	63%	29.11
With Chamber	61%	17.88

Table 3.6: Percentage of sound attenuated within the 300-600 [Hz] frequency range and the average volume of the resonators' necks for the "All resonators" curves in Fig. 3.9c and 3.9d.

We observe the following from Fig. 3.9c and 3.9d: The area under the curve "All resonators" in Fig. 3.9c and Fig. 3.9d in the 300-600 [Hz] range is essentially the same. However, the resonance frequencies of some individual resonators in Fig. 3.9d, specifically resonators 1 and 2, show proportionally a greater up-shift in attenuation coefficient when in the presence of the other resonators and the chamber, compared to the up-shift observed in the resonators in Fig. 3.9c. In Fig. 3.9d we do not observe and up-shift for resonators 3, 4, 5 and 6 because they already reach values above 0.9.

While all resonance frequencies in Fig. 3.9c remain relatively constant whether in presence of the remaining resonators or not, some resonators in Fig. 3.9d, specifically resonators 0, 3, and 4 downshift when in presence of the other resonators. It is important to clarify that the individual resonance frequency of each resonator in Fig. 3.9d was measured with the chamber included in the impedance tube. This was done in order to accurately observe the effects the neighbouring resonators alone had

on the resonator.

We are therefore able to observe frequency pulling in Fig. 3.9d. This could be due to the closeness of the resonance frequencies. However this frequency pulling does not occur in Fig. 3.9c, hinting that the added chamber might have a role in the appearance of this phenomenon. It is also observable that the resonance frequency of resonators 0, 3, and 4 merge into one. This is a sign of frequency locking. Again, despite resonators having similar or even smaller differences between their individual resonance frequencies in Fig. 3.9c, no frequency pulling or locking is to be observed.

Despite both Fig. 3.9c and Fig. 3.9d having a similar CAR, it is directly observable in Table 3.6 that the average volume of the necks in Fig. 3.9b is significantly shorter than that of Fig. 3.9a. Smaller necks up shift resonance frequency. Therefore, despite the chamber not being able to show a significant increase in attenuation within the 300-600 Hz range, it could potentially aid in increasing attenuation at lower frequencies.

4

Summary and conclusions

Our goal was to develop a highly efficient low-frequency broadband attenuation metasurface. Based on our literature review, we identified geometric optimization and the induction of coupling between differently tuned resonators as the most promising approaches for lowering resonance frequencies, extending attenuation bandwidth, and enhancing attenuation efficiency.

A common chamber was designed to induce coupling between the resonators within the unit cell of the metasurface. Results show the occurrence of coupling phenomena such as frequency pulling and frequency locking, which are typically observed in electronic resonators but are applicable here using the electro-mechanical-acoustic analogy model. All chamber dimensions exhibit frequency pulling toward lower frequencies, with the strongest effect occurring in the most extreme instance of a 1 mm chamber depth. This phenomenon is consistent with the goal of maintaining a shallow structure. However, the cumulative attenuation response is significantly reduced with decreasing chamber depth, indicating a potential drawback of this method. To address this issue, we applied geometric optimization with the aim of preserving the beneficial frequency pulling while enhancing the cumulative attenuation response.

We employed geometric optimization using a genetic algorithm with the goal of maximizing the cumulative attenuation response within a target frequency range. Our results indicate that the hexagonal structure reported by Kexin et al. exhibited only a 6% improvement in cumulative attenuation response. However, we observed a 35% increase in the HABW, suggesting a slight reduction in resonance frequency efficiency in exchange for a broader bandwidth.

Finally, we conducted two simulations. In the first, we performed geometric optimization on a hexagonal structure without a chamber, using a genetic algorithm. In the second, we optimized a similar structure with an implemented chamber, while maintaining the same metasurface depth. Optimization resulted in increased CAR and HABW for the structure with a chamber (9.9% and 15.9%, respectively). Similarly, the un-chambered structure displayed increases in CAR and HABW after optimization (8.2% and 35%, respectively).

Comparing the optimized un-chambered model and the optimized chambered model, the former displays a CAR approximately 1% higher than that of the chambered structure. However, the chambered structure's bandwidth was approximately 7% narrower. Despite these results, frequency pulling and locking were observed in the chambered structure, with a maximum resonance frequency decrease of 138 Hz toward lower frequencies. The chambered structure also exhibited increased attenuation coefficients for certain resonance peaks, particularly for resonators 1 and 2, compared to the un-chambered structure's resonators 1, 2, 4, 5, and 6.

Overall, genetic algorithm optimization appears to be an effective approach for expanding bandwidth with a moderate reduction in peak attenuation coefficient at resonant frequencies. Incorporating

a chamber exhibits frequency pulling and locking toward lower frequencies but results in reduced bandwidth. Applying geometric optimization to the chambered structure can help mitigate this reduction in bandwidth while preserving the benefits of frequency pulling and locking.

Incorporating a chamber and applying optimization does not appear to provide significant advantages over optimization alone in terms of bandwidth or CAR. However, the presence of frequency pulling and locking in the chambered structure offers potential for extending the lower frequency range of the CAR. Future research aimed at shifting the attenuation band to lower frequencies without sacrificing metasurface depth or incurring significant reductions in bandwidth or CAR could yield promising results.

Resonator coupling shows promise as a method for enhancing sound attenuation as well as for downshifting resonance frequencies. The coupling phenomenon observed in this study can be explained due to the applicability of the electro-mechanical-acoustic analogy, which has demonstrated validity and utility in describing resonator acoustics. The implementation of a common chamber enhances coupling between resonators, suggesting that its incorporation may be useful in designing metasurfaces with low-frequency attenuation. The geometrical simplicity of the common chamber indicates that its implementation would be cost-effective, and the strongest coupling occurred with the thinnest chamber design, implying that this approach may be suitable for developing compact metasurfaces with efficient low-frequency sound attenuation. Such metasurfaces could have a range of applications, from noise-reducing architectural panels to acoustic screens.

Geometric optimization using genetic algorithms has proven effective for metasurface design. This approach has the potential to enhance design efficiency, especially in cases where resonator geometries become more complex. Further studies could explore alternative algorithms to identify the most effective approach. Additionally, using genetic algorithms for geometric optimization demonstrates significant potential for expanding the bandwidth of acoustic structures, contributing to greater automation in the design process.

Future research could focus on investigating how the common chamber induces coupling and the mechanisms behind its coupling effect. Exploring the effect of the common chamber through the electro-mechanical-acoustic analogy could provide additional insights. Alternatively, the use of alternative geometric shapes for the common chamber may be worth exploring. Additionally, characterizing the mechanical mechanisms underlying the coupling effect induced by the common chamber could be valuable.

As discussed earlier, the common chamber shows promise for extending the metasurface's attenuation spectrum to lower frequencies without increasing surface thickness. A study that prioritizes minimizing attenuation coefficient peaks could determine whether this observation holds true and provide valuable insights into the effectiveness of the common chamber and its potential applications.

References

[1] Kone Tenon Charly et al. "Multi-tonal low frequency noise control for aircraft cabin using Helmholtz resonator with complex cavity". In: *Internoise 2021* (2021). URL: `https://www.researchgate.net/publication/354130902_Multi-tonal_low_frequency_noise_control_for_aircraft_cabin_using_Helmholtz_resonator_with_complex_cavity`.

[2] Juliana Araújo Alves et al. "Low-Frequency Noise and Its Main Effects on Human Health—A Review of the Literature between 2016 and 2019". In: *Applied Sciences* (2020). URL: `https://www.mdpi.com/2076-3417/10/15/5205/html`.

[3] Michael G. Jones Benjamin S. Beck Noah H. Schiller. "Impedance assessment of a dual-resonance acoustic liner". In: *Applied Acoustics* (2015). URL: `https://www.sciencedirect.com/science/article/pii/S0003682X15000134`.

[4] M.H.F.De Salis, D.J.Oldham, and S.Sharples. "Noise control strategies for naturally ventilated buildings". In: *Building and Environment* (2002). URL: `https://www.sciencedirect.com/science/article/pii/S0360132301000476`.

[5] Jorge P. Arenas and Malcolm J. Crocker. "Recent Trends in Porous Sound-Absorbing Materials". In: *Sound and Vibration* (2010). URL: `http://www.sandv.com/downloads/1007croc.pdf`.

[6] Dah-You Maa. "Potential of microperforated panel absorber". In: *Journal of Acoustic Society of America* (1998). URL: `https://asa.scitation.org/doi/pdf/10.1121/1.423870`.

[7] David T. Blackstock. *Fundamentals of Physical Acoustics*. Wiley-Interscience Publication. Wiley, 2000. ISBN: 978-0-471-31979-5.

[8] L. Peng. *Advanced High Strength Natural Fibre Composites in Construction*. Beijing, China: Woodhead Publishing, 2017.

[9] Wolfgang Neise and Lars Enghardt. "Technology approach to aero engine noise reduction". In: *Aerospace Science and Technology* (2003). URL: `https://www.sciencedirect.com/science/article/pii/S1270963803000270`.

[10] Yutao Wu et al. "Deep-subwavelength broadband sound absorbing metasurface based on the update finger coiling-up method". In: *Applied Acoustics* (2022). URL: `https://www.sciencedirect.com/science/article/pii/S0003682X22002201`.

[11] Donald A. Simons. "Reflection of Rayleigh waves by strips, grooves, and periodic arrays of strips or grooves". In: *The Journal of the Acoustical Society of America* (1978). URL: `https://asa.scitation.org/doi/10.1121/1.381881`.

[12] S. R. Seshadri. "Effect of periodic surface corrugation on the propagation of Rayleigh waves". In: *The Journal of the Acoustical Society of America* (1979). URL: `https://asa.scitation.org/doi/10.1121/1.382480`.

[13] Xiaoning Liu and Gengkai Hu. "Elastic Metamaterials Making Use of Chirality: A Review". In: *Journal of Mechanical Engineering* (2016). URL: `http://www.micromechanics.cn/wp-content/uploads/2015/12/Elastic-Metamaterials-Making-Use-of-Chirality-A-Review.pdf`.

[14] Hussein et al. "Dynamics of Phononic Materials and Structures: Historical Origins, Recent Progress, and Future Outlook". In: *Applied Mechanics Reviews* (2014). URL: `https://www.researchgate.net/publication/275379720_Dynamics_of_Phononic_Materials_and_Structures_Historical_Origins_Recent_Progress_and_Future_Outlook`.

[15] Yu Yao et al. "Recent progresses on metamaterials for optical absorption and sensing: a review". In: *Journal of Physics D: Applied Physics* (2021). URL: `https://iopscience.iop.org/article/10.1088/1361-6463/abccf0`.

[16] Godson IVBUOBE. "An Overview of Optical Metamaterials and Future Outlook". In: *Uniport Journal of Engineering and Scientific Research* (2021). URL: `https://www.researchgate.net/publication/353083363_An_Overview_of_Optical_Metamaterials_and_Future_Outlook`.

[17] Zhengyou Liu et al. *Locally Resonant Sonic Materialss*. URL: `https://www.science.org/doi/pdf/10.1126/science.289.5485.1734`. (accessed: 13.09.2022).

[18] Hongfei Zhu, Timothy F. Walsh, and Fabio Semperlotti. "Total-internal-reflection elastic metasurfaces: Design and application to structural vibration isolation". In: *Applied Physics Letters* (2018). URL: `https://aip.scitation.org/doi/pdf/10.1063/1.5052538`.

[19] Xinxin Guo et al. "Manipulating acoustic wave reflection by a nonlinear elastic metasurface". In: *Journal of Applied Physics* (2017). URL: `https://aip.scitation.org/doi/citedby/10.1063/1.5015952`.

[20] Ye Gu et al. "Ultrathin Composite Metasurface for Absorbing Subkilohertz Low-Frequency Underwater Sound". In: *Physical Review Applied* (2021). URL: `https://journals.aps.org/prapplied/abstract/10.1103/PhysRevApplied.16.014021`.

[21] Siddharth Nair, Mehdi Jokar, and Fabio Semperlotti. "Nonlocal acoustic black hole metastructures: Achieving broadband and low frequency passive vibration attenuation". In: *Extreme Mechanics Letters* (2022). URL: `https://www.sciencedirect.com/science/article/pii/S0888327021010359`.

[22] A. Nuñez-Labielle et al. "Towards shock absorbing hyperelastic metamaterial design. (I) Macroscopic scale: Computational shock-capturing". In: *Computer Methods in Applied Mechanics and Engineering* (2022). URL: `https://www.sciencedirect.com/science/article/pii/S0045782522000925?via%3Dihub`.

[23] Guobiao Hu et al. "Acoustic-elastic metamaterials and phononic crystals for energy harvesting: a review". In: *Smart Materials and Structures* (2021). URL: `https://iopscience.iop.org/article/10.1088/1361-665X/ac0cbc/pdf`.

[24] Zhenkun Lin and Serife Tol. "Elastic Metasurfaces for Full Wavefront Control and Low-Frequency Energy Harvesting". In: *Journal of Vibration and Acoustics* (2021). URL: `https://asmedigitalcollection.asme.org/vibrationacoustics/article/143/6/061005/1100529/Elastic-Metasurfaces-for-Full-Wavefront-Control`.

[25] Jun Zhang et al. "Vibration control of flexural waves in thin plates by 3D-printed metasurfaces". In: *Journal of Sound and Vibration* (2020). URL: `https://www.sciencedirect.com/science/article/pii/S0022460X20302728`.

[26] Tian Zhao et al. "Deep-subwavelength elastic metasurface with force-moment resonators for abnormally reflecting flexural waves". In: *International Journal of Mechanical Sciences* (2022). URL: `https://www.sciencedirect.com/science/article/pii/S0020740322001187`.

[27] Andrea Colombi et al. "A seismic metamaterial: The resonant metawedge". In: *Scientific Reports* (2016). URL: `https://www.nature.com/articles/srep27717`.

[28] Lingling Wu et al. "A brief review of dynamic mechanical metamaterials for mechanical energy manipulation". In: *Materials Today* (2021). URL: `https://www.sciencedirect.com/science/article/pii/S1369702120303618`.

[29] Yongdu Ruan, Xu Liang, and Chuanjie Hu. "Retroreflection of flexural wave by using elastic metasurface". In: *Journal of Applied Physics* (2020). URL: `https://aip.scitation.org/doi/full/10.1063/5.0005928`.

[30] Pierre A. Deymier. *Acoustic Metamaterials and Phononic Crystals*. SOLID-STATE SCIENCES. Springer, 2013. ISBN: 978-3-642-31231-1.

[31] Jie Deng et al. "A metamaterial consisting of an acoustic black hole plate with local resonators for broadband vibration reduction". In: *Journal of Sound and Vibration* (2022). URL: `https://www.sciencedirect.com/science/article/pii/S0022460X22000542?via%3Dihub`.

[32] Liyun Cao et al. "Flexural wave absorption by lossy gradient elastic metasurface". In: *Journal of the Mechanics and Physics of Solids* (2020). URL: `https://www.sciencedirect.com/science/article/pii/S0022509620302866`.

[33] Hui Guo et al. "Investigation on acoustic energy harvesting based on quarter-wavelength resonator phononic crystals". In: *Advances in Mechanical Engineering* (2018). URL: `https://journals.sagepub.com/doi/10.1177/1687814017748077`.

[34] Kexin Zeng et al. "Acoustic metamaterial for highly efficient low-frequency impedance modulation by extensible design". In: *Extreme Mechanics Letters* (2022). URL: `https://www.sciencedirect.com/science/article/pii/S2352431622001456`.

[35] Yan Du et al. "Control the structure to optimize the performance of sound absorption of acoustic metamaterial: A review". In: *AIP Advances* (2021). URL: `https://aip.scitation.org/doi/10.1063/5.0042834`.

[36] K. Mahesh and R. S. Mini. "Investigation on the Acoustic Performance of Multiple Helmholtz Resonator Configurations". In: *Acoustics Australia* (2020). URL: `https://link.springer.com/content/pdf/10.1007/s40857-021-00231-8.pdf`.

[37] F. Langfeldt, H. Hoppen, and W. Gleine. "Resonance frequencies and sound absorption of Helmholtz resonators with multiple necks". In: *Applied Acoustics* (2019). URL: `https://www.sciencedirect.com/science/article/pii/S0003682X18306704`.

[38] Haiqin Duan et al. "Acoustic multi-layer Helmholtz resonance metamaterials with multiple adjustable absorption peaks". In: *Applied Physics Letters* (2021). URL: `https://aip.scitation.org/doi/10.1063/5.0054562`.

[39] Xiaodong Zhang et al. "Simultaneous realization of large sound insulation and efficient energy harvesting with acoustic metamaterial". In: *Smart Materials and Structures* (2018). URL: `https://iopscience.iop.org/article/10.1088/1361-665X/aade3e`.

[40] Junzhe Zhu et al. "A multi-layer overlapping structure for continuous broadband acoustic wave absorption at lower-frequencies". In: *Applied Acoustics* (20022). URL: `https://www.sciencedirect.com/science/article/pii/S0003682X21005909?pes=vor`.

[41] Meng Jin et al. "Ultrathin Planar Metasurface-based Acoustic Energy Harvester with Deep Subwavelength Thickness and Mechanical Rigidity". In: *Scientific Reports* (2019). URL: `https://www.nature.com/articles/s41598-019-47649-9`.

[42] Ralf Lucklum. "Phononic crystals and metamaterials - Promising new sensor platforms". In: *Procedia Engineering* (2014). URL: `https://www.sciencedirect.com/science/article/pii/S1877705814023765`.

[43] Hongfei Zhu et al. "On the broadband vibration isolation performance of nonlocal total-internal-reflection metasurfaces". In: *Journal of Sound and Vibration* (2022). URL: `https://www.sciencedirect.com/science/article/pii/S0022460X21006829?via%3Dihub`.

[44] Yong Li and Badreddine M. Assouar. "Acoustic metasurface-based perfect absorber with deep subwavelength thickness". In: *Applied Physics Letters* (2016). URL: `https://aip.scitation.org/doi/full/10.1063/1.4941338`.

[45] Krupali Donda, Yifan Zhu, and Shi-Wang Fan. "Extreme low-frequency ultrathin acoustic absorbing metasurface". In: *Applied Physics Letters* (2019). URL: `https://aip.scitation.org/doi/pdf/10.1063/1.5122704`.

[46] Zhiwen Ren et al. "A compact multifunctional metastructure for Low-frequency broadband sound absorption and crash energy dissipation". In: *Materials Design* (2022). URL: `https://www.sciencedirect.com/science/article/pii/S0264127522000831?via%3Dihub`.

[47] Lei Zhang and Fengxian Xin. "Perfect low-frequency sound absorption of rough neck embedded Helmholtz resonators". In: *The Journal of the Acoustical Society of America* (2022). URL: `https://asa.scitation.org/doi/pdf/10.1121/10.0009529`.

[48] D. Roca et al. "Multiresonant Layered Acoustic Metamaterial (MLAM) solution for broadband low-frequency noise attenuation through double-peak sound transmission loss response". In: *Extreme Mechanics Letters* (2021). URL: `https://www.sciencedirect.com/science/article/pii/S2352431621001152?via%3Dihub`.

[49] Hongfei Zhu et al. "Nonlocal elastic metasurfaces: Enabling broadband wave control via intentional nonlocality". In: *Engineering* (2020). URL: `https://www.pnas.org/doi/10.1073/pnas.2004753117`.

[50]   Zhiling Zhou et al. "Broadband impedance modulation via non-local acoustic metamaterials". In: *National Science Review* (2021). URL: `https://academic.oup.com/nsr/article/9/8/nwab171/6368878`.

[51]   Sibo Huang, Xinsheng Fang, and et al. Xu Wang. "Acoustic perfect absorbers via spiral meta-surfaces with embedded apertures". In: *Applied Physics Letters* (2018). URL: `https://aip.scitation.org/doi/10.1063/1.5063289`.

[52]   Giuseppe Bertuccio. "On the physical origin of the electro-mechano-acoustical analogy". In: *The Journal of the Acoustical Society of America* (2022). URL: `https://pubs.aip.org/asa/jasa/article/151/3/2066/2838334/On-the-physical-origin-of-the-electro-mechano`.

[53]   Mingyu Duan et al. "Acoustic impedance regulation of Helmholtz resonators for perfect sound absorption via roughened embedded necks". In: *Applied Physics Letters* (2020). URL: `https://pubs.aip.org/aip/apl/article-abstract/117/15/151904/39269/Acoustic-impedance-regulation-of-Helmholtz?redirectedFrom=fulltext`.

[54]   Sibo Huang et al. "Compact broadband acoustic sink with coherently coupled weak resonances". In: *Science Bulletin* (2020). URL: `https://www.sciencedirect.com/science/article/pii/S2095927319306401`.

[55]   Behzad Razavi. "A Study of Injection Locking and Pulling in Oscillators". In: *IEEE JOURNAL OF SOLID-STATE CIRCUITS* (2004). URL: `http://www.seas.ucla.edu/brweb/papers/Journals/RSep04.pdf`.

[56]   COMSOL. *Acoustics Module User's Guide*. English. COMSOL. June 3, 2023. 680 pp. final.